Pergamon

Deep-Sea Research II, Vol. 44, No. 9–10, pp. 1827–1849, 1997

Printed in Great Britain

PII: S0967-0645(97)00031-3

0967-0637/98 $19.00 + 0.00

A meeting place of great ocean currents: shipboard observations of a convergent front at 2°N in the Pacific

DAVID ARCHER,* JIM AIKEN,† WILLIAM BALCH,‡ DICK BARBER,§ JOHN DUNNE,¶ PIERRE FLAMENT,‖ WILFORD GARDNER,** CHRIS GARSIDE,‡ CATHERINE GOYET,†† ERIC JOHNSON,‡‡ DAVID KIRCHMAN,§§ MICHAEL MCPHADEN,¶¶ JAN NEWTON,¶ EDWARD PELTZER,†† LEIGH WELLING,‖‖ JACQUES WHITE*** and JAMES YODER†††

(*Received* 13 *May* 1997; *accepted* 9 *July* 1997)

Abstract—We present a synthesis of physical, chemical and biological shipboard observations of a convergent front at 2°N, 140°W and its surrounding environment. The front was a component of a tropical instability wave generated by shear between westward-flowing equatorial waters to the south and warmer equatorial counter current water to the north. Surface waters on the cold side were undersaturated with oxygen, which suggests that the water had only been exposed at the sea surface for a period of a few weeks. Although the atmospheric exposure time was short, the effects of biological activity could be detected in enhanced concentrations of total (dissolved plus suspended particulate) organic carbon concentration, proving that TOC can be produced quickly in response to changing environmental conditions. The front itself was dominated by the accumulation of a "patch" of buoyant diatoms *Rhizosolenia castracanei* concentrated in the top centimeters of the warm surface water north of the front, and elevated chlorophyll concentrations were observed from the air over a spatial scale of order 10–20 km northward from the front. The nitrogen budget and thorium data suggest that a significant fraction of the elevated POC, and virtually all of the PON, arrived in the patch waters as imported particles rather than *in situ* photosynthesis. Photosynthetic uptake of carbon appears to have occurred in patch waters, but without corresponding uptake of fixed nitrogen (an uncoupling of the usual Redfield stoichiometry). Solute chemistry of the patch appears to be controlled by turbulent mixing, which flushes out patch waters on a time scale of days

* Department of the Geophysical Sciences, University of Chicago, Chicago, IL 60637, U.S.A.

† Plymouth Marine Laboratory, Plymouth Pl1 3DH, U.K.

‡ Bigelow Laboratory for Ocean Science, McKown Point, West Boothbay Harbor, ME 04575, U.S.A.

§ Duke University Marine Laboratory, Pivers Island, Beaufort, NC 28516, U.S.A.

¶ School of Oceanography, WB-10, University of Washington, Seattle, WA 98195, U.S.A.

‖ Department of Oceanography, University of Hawaii, Manoa, 1000 Pope Road, Honolulu, HI 96822, U.S.A.

** Department of Oceanography, Texas A&M University, College Station, TX 77843, U.S.A.

†† Department of Chemistry, Woods Hole Oceanographic Institution, Woods Hole, MA 02543, U.S.A.

‡‡ Joint Institute for the Study of the Atmosphere and Oceans, University of Washington, Seattle, WA 98195, U.S.A.

§§ College of Marine Sciences, University of Delaware, Lewes, DE 19958, U.S.A.

¶¶ Pacific Marine Environmental Laboratory, NOAA, 7600 Sand Point Way NE, Seattle, WA 98115, U.S.A.

‖‖ College of Oceanography, Oregon State University, Corvallis, OR 97331, U.S.A.

*** People for Puget Sound, 1326 5th Avenue, Seattle, WA 98101, U.S.A.

††† Graduate School of Oceanography, University of Rhode Island, Narragansett Bay Campus, Narragansett, RI 02882, U.S.A.

(faster than atmospheric ventilation). The subduction of nutrient-rich equatorial surface water below the front was detected 100 km north of the front in the signatures of temperature, salinity and ammonium.

INTRODUCTION

"At seven-thirty, after sounding, temperatures, and breakfast, I went on the bridge and saw a very distinct line in the water to the north. The captain said we had been steaming parallel to it since dawn. I had the *Arcturus* turned toward it at once, and found the Sargasso Sea of the Pacific, only in this instance it was a wall of water, against which all the floating jetsam for miles and miles was drifted and held. . . . When we first detected the rip we were in 2°36′ North Latitude, and 85° West Longitude, which placed us about two hundred miles southeast of Cocos Island.

When I approached within the possibility of more accurate examination, I saw that the line, which stretched from horizon to horizon, extended in a northeast and southwest direction. On our side, the south, the water showed dark and rough, but much lighter and smoother to the north. When the *Arcturus* was at last actually astraddle of the rip, I saw it as a narrow line of foam, zigzagging across the placid sea, with spouting white-caps shooting up through the froth that marked the meeting place of the great ocean currents."

The journey of the *Arcturus* was sponsored by the National Zoological Society of America and took place in 1925. William Beebe's description of a convergent front in April at 2°N, 85°W in the eastern Pacific was first published in 1926 (Beebe, 1926) and yet sounds astonishingly familiar to participants in the JGOFS Fall Survey expedition of August–September 1992. A photograph published in Beebe's account is indistinguishable from a photograph taken on the JGOFS cruise (Yoder *et al.*, 1994; Fig. 1).

As in Beebe's time, our initial detection of the front came from the officers on the bridge, in our case via radar where the front appeared as a distinct line of high reflection. Our position was 140°W, 2°N, considerably west of Beebe's report. The radar showed a line of choppy seas associated with the outcropping density stratification and current shear of the front. In addition to the breaking waves the front was marked by a surface "patch" of buoyant diatoms *Rhizosolenia castracanei* (Yoder *et al.*, 1994). The *Rhizosolenia* patch generated a striking contrast in sea surface color across the front. The south (cold) side was dark blue, whereas the north (warm) side (containing the *Rhizosolenia* patch) was a yellowish–green mixture of the colors of hay and split pea soup. The *Rhizosolenia* patch was quite shallow; aft of the moving ship, the patch was swept aside by the wake revealing blue water underneath.

The dynamics of the front were intimately associated with upwelling at the equator and shear between the westward flowing South Equatorial Current and the eastward North Equatorial Counter Current. Shear instability generates a sawtooth-shaped fluctuation in the boundary between the two currents, which propagates westward with a period of 25–30 days (Legeckis, 1977; Kessler and McPhaden, 1995; Flament *et al.*, 1996; Johnson, 1996; McPhaden, 1996). Superimposed upon the instability wave is the divergence-driven upwelling of water at the equator, which drives subduction to the north. The convergent front was located on the westward (leading) edge of the instability wave.

Here we present a summary of numerous investigators' shipboard and remote observations of the wave and front to reconstruct its impact on the chemistry and biology of the equatorial surface ocean. Shipboard data comes from two 140°W Survey legs of the

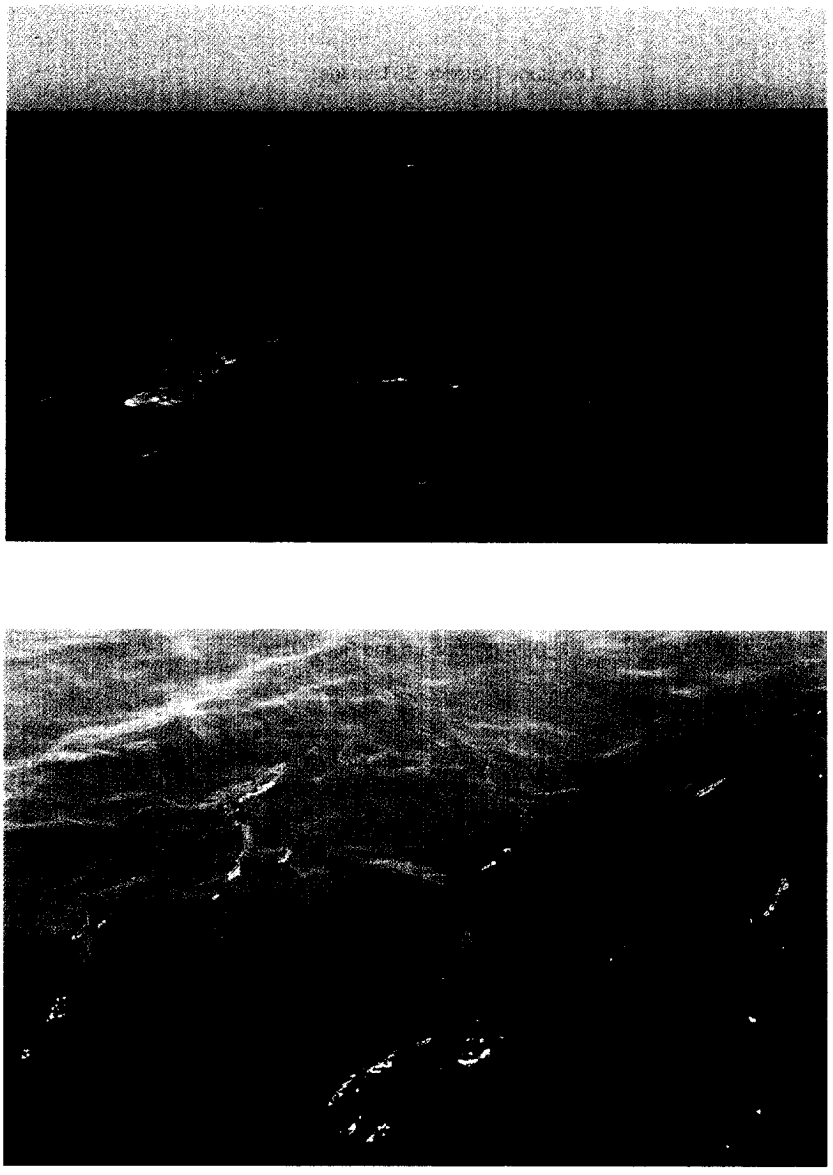

Fig. 1. A photograph of the convergent front from RV *Thompson*.

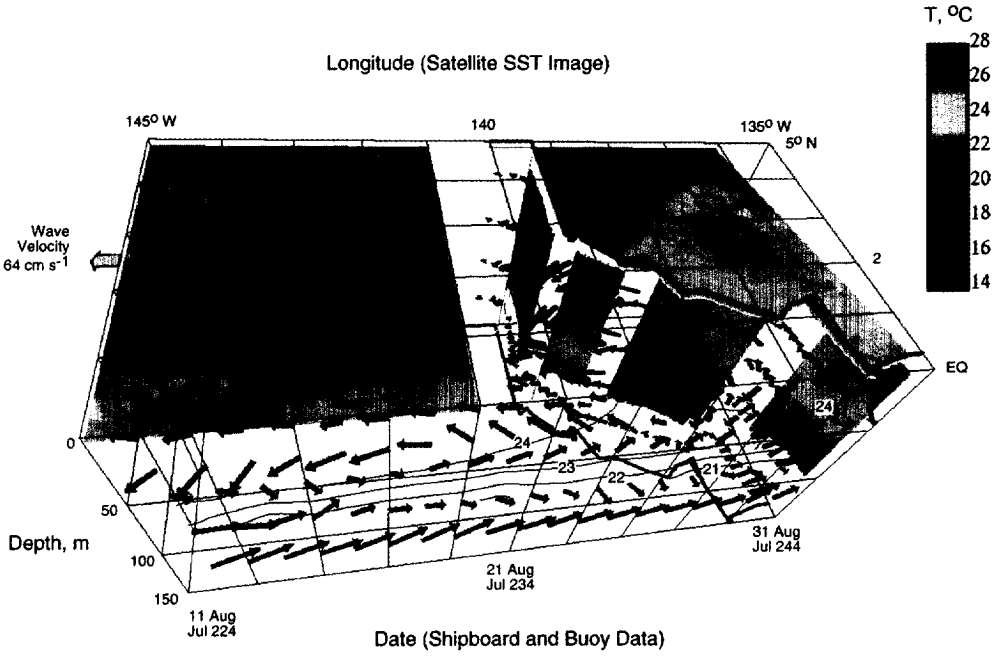

Fig. 2. A synthesis of temperature observations. A sea surface temperature swath from the NOAA AVHRR satellite (Flament *et al.*, 1996) is cut away to reveal sub-surface detail from shipboard and moored observations. The satellite image was taken on 21 August, while the ship was at 5°N. To correct for the westward propagation of the wave while we made our way down to the equator, the shipboard and moored data has been transposed to the east at a rate of 0.5° per day from 21 August (Julian day 234, 0000 GMT). The convergent front described by Yoder *et al.* (1994) can be seen as the diagonal line in SST, reaching from about 140°W at the equator to 135°W and 5°N. The satellite image is cut away to reveal continuous temperature sections from the surface to approximately 100 m depth, generated using an Undulation Oceanographic Recorder (UOR, Aiken and Bellan, 1990). Velocity estimates come from shipboard (Johnson, 1996; blue vectors) and moored (Kessler and McPhaden, 1995; red vectors) acoustic doppler current profiler (ADCP) data. Horizontal velocities only are shown; i.e. all vectors are in planes parallel to the sea surface. For scale, a vector the length of 1° (the squares on the surface) would have a magnitude of 333 cm s^{-1}. North of the front, the water flows parallel to the front toward the southwest. Just south of the front the water flows into the front, subducting to the northwest. Near the equator, surface water was flowing to the west, with the equatorial undercurrent flowing eastward.

U.S. JGOFS EqPac expeditions (Murray *et al.*, 1995), which encountered ENSO conditions during Survey I in February–March 1992 and cooler conditions, and the wave and front during Survey II in August–September 1992. We also show data from a PROTEUS mooring at 0°N, 140°W (Kessler and McPhaden, 1995) and from NASA aircraft (Yoder *et al.*, 1994), contemporary with the shipboard observations of the front. The reader is directed to a series of primary papers, mostly contained in the first two Equatorial Pacific JGOFS *Deep-Sea Research* special issues, for details and methodology for the data presented here.

WAVE-SCALE STRUCTURE

Physical description

A synthesis of the temperature and velocity structure of the instability wave was constructed from shipboard, moored and satellite observations (Fig. 2). Synoptic sea surface temperature comes from AVHRR satellite image from 21 August 1992 (Sawyer and Flament, 1995). The front can be seen as the contrast in SST which distinguishes the southeast corner of the image from the rest of the field. On this date, the RV *Thomas G. Thompson* was at 5°N and heading south toward the mooring at the equator. The ground-based shipboard and mooring data are combined with the satellite image of the westward propagating instability wave by transposing the ground data eastward from the 21 August position at a rate of $0.5° \, d^{-1}$ (time is indicated at the bottom of the front face of Fig. 2, Flament *et al.*, 1996; Johnson, 1996). The technique uses time-dependent observations at a single line of longitude as a proxy for zonal structure, based on the assumption that the instability wave is an unchanging feature propagating at a constant velocity. Any real E–W slope of the thermocline will be neglected by the technique, as will time variability of the wave structure.

The satellite image is cut away to reveal high-resolution sub-surface temperature data from a towed undulating optical recorder (UOR), which profiles from near the surface to 100 m depth on a spatial scale of approximately 3 km while the ship is underway. The sea surface front is revealed to be a wedge of warm water to the north. The velocity structure of the water column was characterized by two accoustic doppler current profilers (ADCPs), one aboard the *Thompson* (blue arrows) and the other mounted on the mooring (Kessler and McPhaden, 1995; red arrows). Both shipboard and mooring data are time averaged, and are displaced longitudinally as a function of time. The instability wave is itself propagating to the west, as indicated by the yellow arrow on the left side of the figure. The velocity vectors from shipboard and moored ADCP do not include this component of the wave's velocity; that is to say, they are velocities relative to the earth's surface, rather than relative to the moving front.

North of the front the water flows in a jet roughly parallel to the front, toward the southwest. On the south side of the front the flow is northward, subducting under the warmer waters to the north (Johnson, 1996). The equatorial undercurrent can be seen as eastward sub-surface flow on the front plane of the figure (the equator). At the equatorial sea surface, the coldest waters are seen to the east of the front as the outcropping of the 24° isotherm.

The relationships between the water masses associated with the front can be seen in a temperature/salinity diagram (Fig. 3) (see also Johnson, 1996 and Balch and Kilpatrick, 1996). A T–S trace of a vertical cast on the warm side of the front begins in warm surface

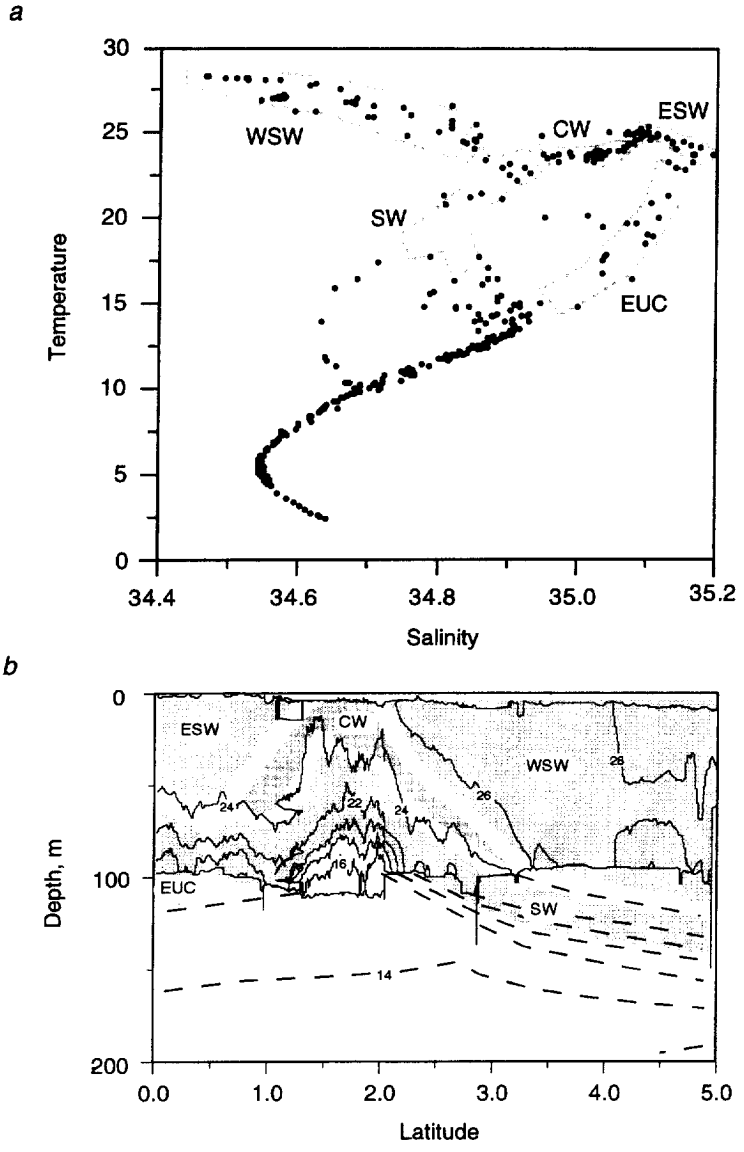

Fig. 3. (a) A T–S diagram of Survey II CTD data from the equator to 5°N. (b) A composite temperature section from UOR data in approximately the upper 100 m (Aiken and Bellan, 1990) and CTD temperature data below that. Shaded regions on both figures correlate the locations of five water masses in T–S space and physical space. Water with a distinctive signature in T–S (a "cusp", sub-surface salinity maximum at temperature of approximately 24°, labeled "CW") outcrops to the south of the front (revealed by the outcropping of the 26° isotherm), and can be traced northward to 3°N in the CTD data. Other water masses have been called warm surface water ("WSW"), equatorial undercurrent ("EUC"), saddle water ("SW") and equatorial surface water ("ESW").

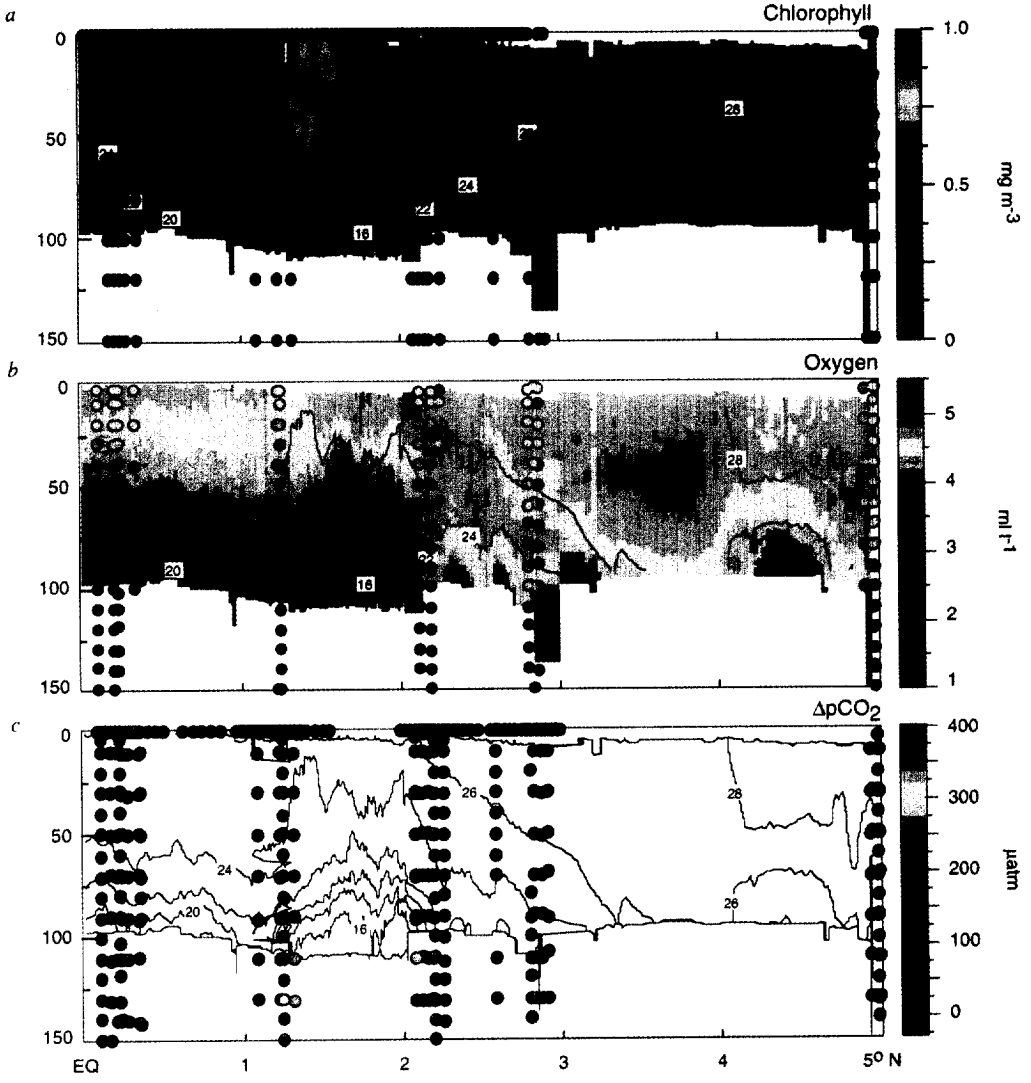

Fig. 4. Sections of (a) chlorophyll (from fluorescence), (b) oyxgen, and (c) pCO_2 from 1° to 5°N, with overlays of temperature contours from UOR. Chlorophyll data come from UOR (Aiken and Bellan, 1990) and underway sampling (Balch and Kilpatrick, 1996). A sub-surface maximum is seen across the entire section, with greatest intensity at around 1°N. The 1°N maximum was also detected in the continuous underway chlorophyll determinations at the sea surface, but was missed entirely by the CTD profiles. Oxygen data (b) come from UOR (Aiken and Bellan, 1990) and CTD section. pCO_2 data come from CTD section (Archer *et al.*, 1996) and continuous underway determinations (Goyet and Peltzer, submitted).

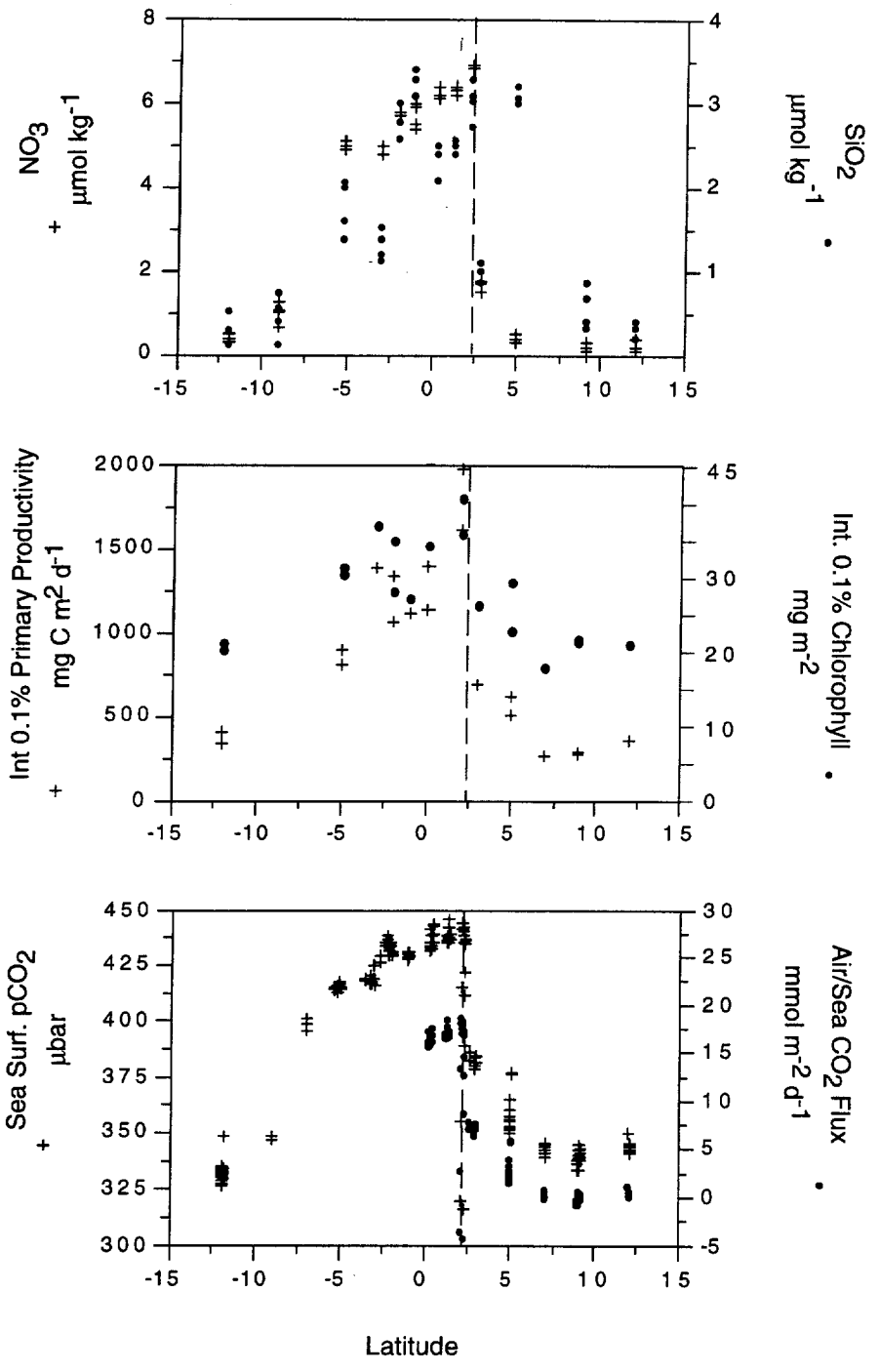

Fig. 5. (a) Nutrient concentrations (Garside and Garside, 1995), (b) primary productivity (Barber *et al.*, 1996) and integrated chlorophyll concentrations and (c) CO_2 concentrations and fluxes from Survey II (Archer *et al.*, 1996). All these properties had maximum values south of the front at 2°N.

water at relatively low salinity. With increasing depth the trace ventures toward the T–S signature of equatorial surface water with higher salinity, and below that, the salinity trend reverses, decreasing into deep water. This distinctive salinity reversal "cusp" signature can be seen in sub-surface waters to the north, suggesting a relationship between cold surface waters at 2°N and sub-surface waters at 3°N. A similar T–S cusp is visible in Survey I data, but the cusp water during Survey I never outcropped. In T–S space, the cusp water appears to be related to equatorial surface water, although neither cusp water nor waters from the T–S "saddle" beneath the cusp water can be found at the equator, presumably due to dominance of the equatorial undercurrent on the provenance of waters in the 100–150 m depth range.

Chemistry and biology

The wave and the front had profound impacts on the biology and chemistry of the water column. The correspondence of chlorophyll, oxygen and pCO_2 with the temperature structure of the wave can be seen in UOR and shipboard analyses (Fig. 4). A sub-surface maximum of chlorophyll is seen throughout the entire 5° of the transect (Fig. 4a), with particularly high values between 1° and 2°N. A sea surface expression of the 1°–2°N feature was detected in the underway sea surface chlorophyll determinations by Balch and Kilpatrick (1996), but missed by the CTD sampling program. Shipboard oxygen (Murray *et al.*, 1995; Fig. 4b) and pCO_2 data (Fig. 4c; Archer *et al.*, 1996; Goyet and Peltzer, submitted) reveal the profound and abrupt transition in water chemistry between the warm waters to the north and the colder southern waters.

Cold waters south of the front. The cold surface waters south of the front are denser than equatorial surface water and are, in fact, the densest surface waters observed during either JGOFS Survey transect. Consistent with the general increase in nutrient concentration and pCO_2 with density in the ocean, this water predictably had high concentrations of nutrients and high pCO_2 (Fig. 5). The exposure of fertile sub-surface water to the atmosphere is presumably the cause of the highest measured rate of primary production and calculated rate of air–sea gas exchange from the transects. Above and beyond this observation, we can say from relationship between oxygen and CO_2 at the sea surface (Fig. 6) that this water has only been exposed to the atmosphere for a short time (Archer *et al.*, 1996). A simple model for simultaneous gas exchange of oxygen and CO_2, beginning with initial conditions from sub-surface waters, constrains the maximum atmospheric exposure time of these waters to 10–20 days. Apparently the mixed layer is either subject to intense mixing with sub-surface waters or else the entire mixed layer is flushed through by ventilation along an outcropping isopycnal surface. Current velocities from ADCP are consistent with this short atmospheric exposure time: the average northward velocity of surface waters between the equator and 2°N was 45 cm s^{-1}, which should cover the 220 km distance in 6 days.

Exposure of thermocline waters to the atmosphere was clearly responsible for high values of pCO_2 and CO_2 evasion rates from the ocean. Beyond this, however, subduction of nutrient-rich waters is a process that has special significance to understanding the dynamics of the carbon cycle in the thermocline. Consider a parcel of water at the sea surface, with zero nutrients and in atmospheric equilibrium in CO_2. The parcel is subducted and gains nutrients and CO_2 by oxidation of biological particles sinking from above. If this parcel is brought to the surface again and held there until biological activity has depleted the nutrient

stock completely, the excess CO_2 typical of thermocline water is incorporated into biogenic particles and pumped to depth, resulting in zero net flux to the atmosphere (neglecting any temperature change and its effect on CO_2 solubility). If, on the other hand, the parcel is exposed to the atmosphere and allowed to degas, but subducted before its nutrients are completely utilized, a net flux of CO_2 from the thermocline to the atmosphere is allowed to occur. In other words, ventilation and subduction of high-nutrient waters may constitute a

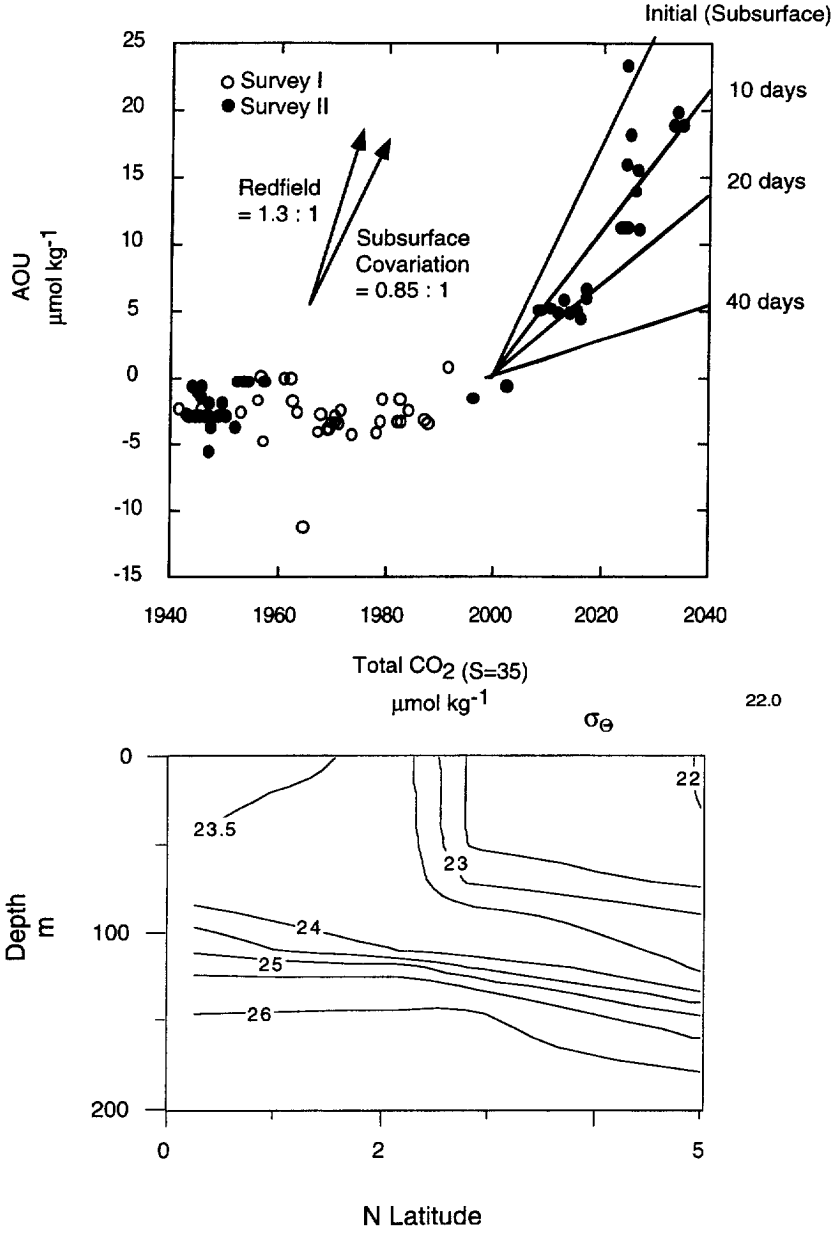

"leak" of biological pump CO_2 from the thermocline to the atmosphere, relative to the case of complete nutrient utilization. Our data show that the intense dynamics of the front drive subduction of nutrients in spite of anomalously high rates of particulate primary and export production on the outcropping cold waters.

DOM production resulting from surface exposure. A major uncertainty in our understanding of the carbon cycle in the upper ocean is the role of dissolved organic matter (DOM), the rate of production of which is poorly known. DOM concentration variability was characterized by measuring total organic carbon (TOC) by injecting unfiltered seawater samples into a high temperature organic carbon analyzer (Peltzer and Hayward, 1996). Figure 7 shows the relationship between the dissolved plus particulate organic carbon concentration, TOC, and s_q between the equator and 5°N from both Survey I and II transects. At s_q between 22.5 and 24 (characteristic of the outcropping water on the cold side of the front during Survey II, see shading in Fig. 7) the TOC concentration is elevated relative to Survey I data. We surmise that the TOC concentration responded to biological activity at the sea surface, within the 10–20 day time frame of atmospheric exposure (Fig. 6). In contrast, the pCO_2 and nutrient concentrations when plotted against density are indistinguishable between Survey I and Survey II, except for waters within the *Rhisosolenia* patch (Archer *et al.*, 1996). One definition of a long-lived chemical species in the ocean would be one whose production and decay times are comparable with the circulation time of the ocean, whereas a transient tracer might by definition have a lifetime which is shorter than the ocean circulation. Here we show a component of TOC which is clearly transient by this definition.

Fig. 6. (a) Sea surface (< 30 m) oxygen vs total CO_2 normalized to a salinity of 35. (b) Density sections from the equator to 5°N. Data from the shaded region of (a) were from Survey II from 2°N to the equator, as indicated by the shaded region of (b). Oxygen data serves as a tracer for the atmospheric exposure time of surface waters on the cold side of the front. Oxygen is plotted as apparent oxygen utilization (AOU), the deviation from saturation at 1 atm total pressure, with positive AOU denoting undersaturation. Sub-surface waters in this region covary in their oxygen: total CO_2 concentrations in a ratio of -0.85:1, as indicated by the vector [the deviation from Redfield is due to the export of $CaCO_3$ and increasing solubility of CO_2 in colder waters (Archer *et al.*, 1996)]. On exposure to the atmosphere, both oxygen and CO_2 will begin to equilibrate toward atmospheric saturation values. Given a gas exchange rate constant, k, the gas exchange rate of oxygen can be calculated as

$$\text{Flux } CO_2 \text{ (mol m}^{-2} \text{ d}^{-1}) = k \text{ (m d}^{-1}) \times \Delta O_2 \text{ (mol m}^{-3})$$

where k is an exchange coefficient, and DO_2 is the deviation from oxygen saturation. For total CO_2, the exchanging species is $CO_{2(aq)}$, which has a concentration very much smaller than the total dissolved CO_2 concentration (which includes HCO_3^- and $CO_3^=$). Under conditions of constant temperature and alkalinity, the exchange flux of CO_2 can be calculated from the total CO_2 concentration as

$$\text{Flux } CO_2 \text{ (mol m}^{-2} \text{ d}^{-1}) = k \text{ (m d}^{-1}) \times \gamma \times \Delta \sum CO_2 / \sum CO_{2ref} \times [CO_2]_{(aq)ref}$$

where γ is the Revelle buffer factor, taken for the cold water to be 12 (Archer *et al.*, 1996), $DSCO_2$ is the deviation of total CO_2 of the saturation value, ΣCO_{2ref} (taken here to be 1990 μM kg^{-1}), and $[CO_2]_{(aq)\ ref}$ is the dissolved CO_2 gas concentration at atmospheric saturation, taken here to be 10.2 μM kg^{-1}. The mixed-layer depth varied diurnally between 15 and 40 m from the equator to 1°N, and increased to 10–70 m diurnally in the cold water just south of the front. For this calculation we assume an average of 60 m. The diagonal lines in the shaded region indicate the time evolution of the total CO_2/oxygen signature of a suite of recently exposed surface waters. The initial ratio of total CO_2/oxygen variability is labeled "Initial (Subsurface)". In the course of time, the faster equilibration of oxygen drives the co-variation toward a flat ratio, as observed in the rest of the Survey I and II datasets. We conclude the surface exposure time was of the order of 10–20 days.

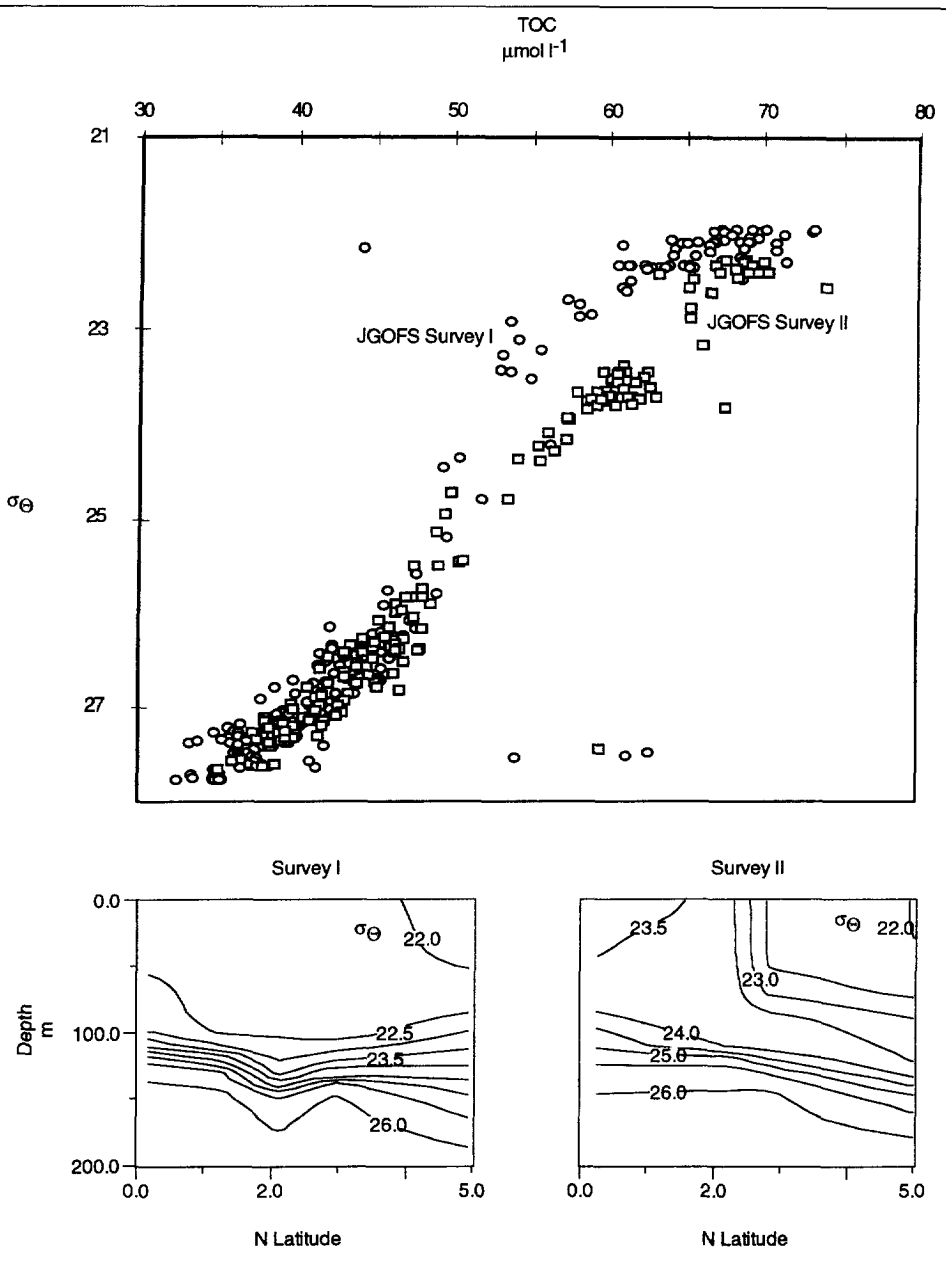

Fig. 7. Total organic carbon (TOC) as a function of σ_θ from Survey I and II (Peltzer and Hayward, 1996; Archer *et al.*, 1997). Survey II data (squares) with $22.5 < \sigma_\theta < 24$ is elevated by approximately 10 µmol kg^{-1} relative to Survey I (circles). As noted in the lower panels, water of this density was between 60 and 120 m during Survey I, but reached the surface from the equator to 2°N, where it was subducted. It is likely that exposure to the euphotic zone during Survey II results in the elevated TOC levels. The short exposure time of this water to the sea surface (10–20 days; Fig. 6) implies that TOC responds quickly to biological forcing.

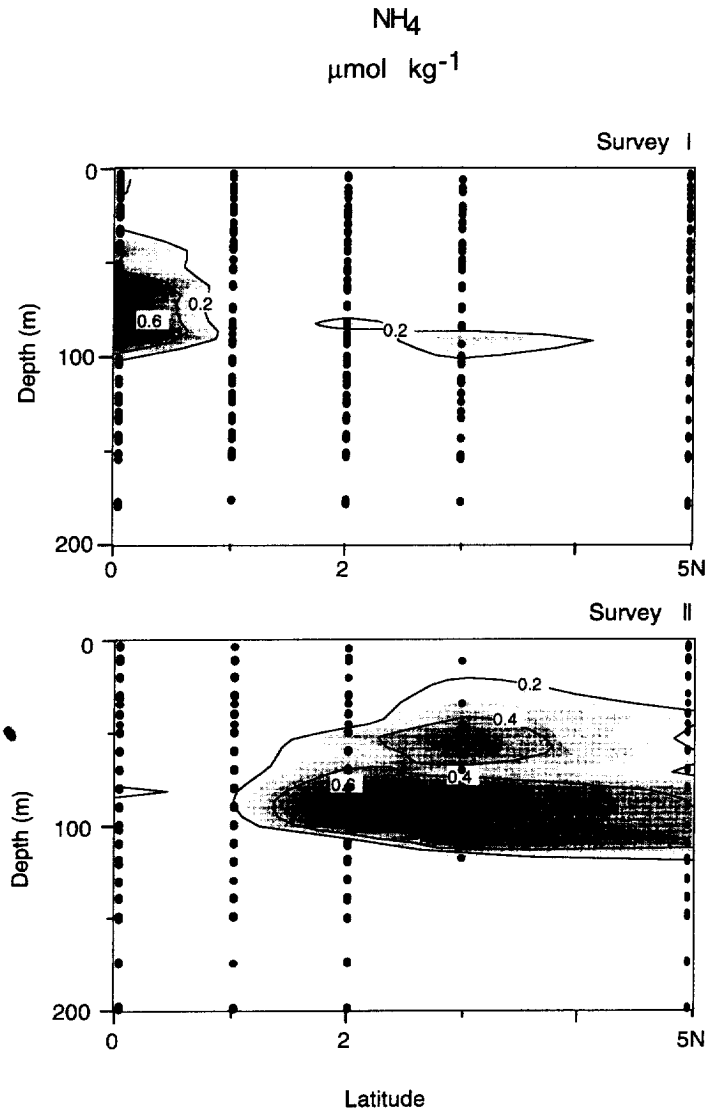

Fig. 8. Sections of NH_4, composited from data by Garside and Garside (1995) and McCarthy *et al.* (1996). Subducting "cusp" water (Fig. 3) shows elevated concentrations of this indicator of microbial activity, while this watermass outcropped during Survey II but not during Survey I.

Signatures of ventilation in sub-surface waters. In addition to the sub-surface signatures found in surface water south of the front, we detected the signature of surface exposure within the waters beneath the sea surface north of the front. These include a maximum in NH_4 (Garside and Garside, 1995; McCarthy *et al.*, 1996) found in "cusp" water (refer to Fig. 3), which was present in Survey II but absent in Survey I (Fig. 8). This signal might be attributed to local production north of the front, but rates of primary production and particle export at 3° and 5°N were similar between Survey I and II. The more plausible

explanation is that the NH_4 maximum was generated by subduction and oxidation of suspended particulate and dissolved organic matter (i.e. TOC) that was produced at or south of the convergent front. The mesozooplankton biomass was elevated at depth in the ammonium maximum at 3°N relative to Survey I observations (Zhang *et al.*, 1995), consistent with local subsurface organic carbon regeneration. In addition, the signature of the radiolarian population assemblage observed at depth at 3°N was characteristic of the cold surface water (Welling *et al.*, 1996).

Mean regional impact of instability waves. The net mean effect of instability waves on the geochemistry of the equatorial Pacific is difficult to judge. The mean rate of equatorial upwelling and poleward subduction is probably determined by forcing from the winds, while the impact of the instability waves would be to modulate the upwelling rate about the wind-determined mean value (Harrison, 1996). A guess about the effect of the waves on the ventilation of the thermocline would, therefore, require a comparison of an ocean with intermittant sea surface exposure of extremely high pCO_2 waters against an ocean with steady exposures of moderately high pCO_2 waters. The net impact of the waves could be either to increase or decrease the ventilation of the thermocline relative to a more sluggish ocean. The effect of the waves on plankton ecology is more definite; an ocean with a high degree of outcropping variability would probably have a more dynamic "bloom selected" ecosystem structure than would a more sluggish ocean. Our geochemical data indicate that the plankton communities observed between the equator and the front must have been only recently exposed to sunlight.

FRONT SCALE STRUCTURE

The subduction of colder fluid from the south side of the front apparently left behind a narrow "patch" of buoyant diatoms *Rhizosolenia castracanei* concentrated in the top few centimeters on the warm side of the front. Beneath the patch and extending much further from the front, the mixed layer exhibited anomalous signatures in chlorophyll, oxygen, CO_2, TOC and POC but, strikingly, not NO_3. An attempt to accommodate all of the data simultaneously allows us to put tight constraints on the physical, chemical and biological dynamics of the frontal system.

Physical structure

The physical structure of the front zone (± 15 km) is summarized in Fig. 9, generated from shipboard ADCP, CTD and UOR data. The section is constructed by arranging the shipboard data according to its distance normal to the front, based on the geometric reconstructions of (Johnson, 1996) and assuming along-front homogeneity. Velocity vectors are shown relative to the front, such that cross-front velocities are in the plane of the section, and along-front velocities are shown extruding from the page. In contrast to Fig. 2, the velocities are presented relative to the moving front by adding an eastward velocity of 64 cm s^{-1} (Johnson, 1996) to the shipboard composite data. The colored line near the sea surface represents composited temperature observations from the ADCP thermister, and the sub-surface temperatures are from CTD deployments.

Sub-surface, the slope of the deepening isothermal surfaces north of the front is not well resolved, but we estimate from the UOR data a slope of approximately 1 m depth per

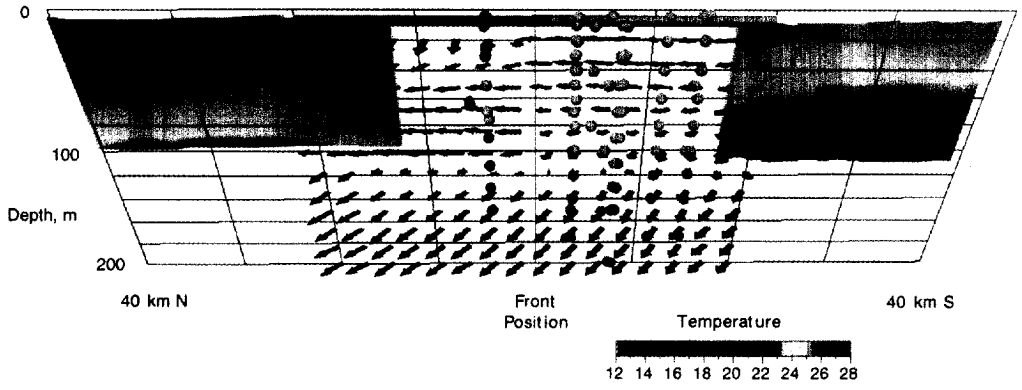

Fig. 9. Physical structure of the convergent front, in section perpendicular to the front. The vectors are from a composite flow field from ten crossings of ADCP data gridded relative to the position of the front, determined by the ADCP sea surface thermister (indicated by the colors of the line at the sea surface) from Johnson (1996). The sub-surface temperatures are from shipboard CTD data arranged as distance perpendicular to the front using the positions determined by Johnson (1996). The continuous temperature sections to either side of the front are from UOR data (Aiken and Bellan, 1990).

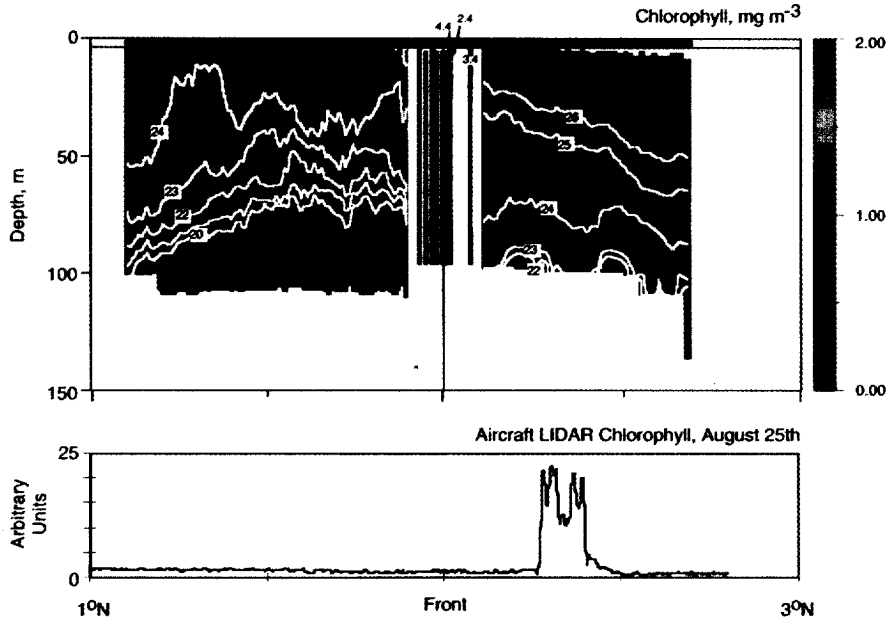

Fig. 10. (a) Chlorophyll distribution (from fluorescence) near the front and in the *Rhizosolenia* patch. The location of the patch is arbitrarily taken here to be 2.00°N, and all data are plotted relative to this. Vertical bars near the patch are from CTD fluorometer data, horizontal bar at the sea surface is from continuous flow-through analysis (Balch and Kilpatrick, 1996), and sections on either side of the front are from UOR (Aiken and Bellan, 1990). The patch chlorophyll concentration ranged from 2.4 to 4.4 mg m^{-3}, and extended to the depth of the patch mixed layer. The actual *Rhizosolenia* mat was buoyant enough to be confined within a few centimeters of the sea surface, and is not resolved by any of these techniques. (b) Aircraft LICF (laser induced chlorophyll fluorescence) at 140°W, taken on 25 August.

kilometer distance. The incoming UOR transect from the north is estimated to end at roughly 11 km north of the front based on the analysis of front movement by Johnson. The proximity of the outgoing transect to the front is more difficult to estimate, because the location of the front with time became less predictable toward the end of our occupation of Station 6 (Eric Johnson, personal communication). Cross-front velocities were to the north, at the surface south of the front and continuing sub-surface north of the front at a rate of roughly 20 cm s^{-1} averaged over a depth interval of about 100 m. From this we can calculate a subduction rate of 20 m^3 s^{-1} per linear meter of the front; if this flow were characteristic of values along a homogeneous 500 km front, we would calculate a subduction rate of approximately 10 Sv over a single wavelength of the tropical instability wave train. This can be compared with an estimate of a 50 Sv of upwelling and equatorial divergence over the entire equatorial region, 5°N–5°S, dateline to 90°E (Wyrtki, 1981).

Chemical and biological observations

A high-resolution section of chlorophyll concentration across the front was assembled from shipboard UOR, sea surface continuous analysis (Balch and Kilpatrick, 1996) and CTD fluorescence data (Fig. 10). Note that the *Rhizosolenia* patch, isolated to the top few centimeters of the sea surface, was missed by the flow-through and CTD data, which recorded instead characteristics of the bulk mixed layer composition, refered to here as warm frontal water. The location of the front is arbitrarily taken to be at 2.00°N, and all data are plotted relative to this. The CTD fluorescence data are plotted relative to the distance from the front using the cruise track geometry from Johnson (1996) (Table 1). Fluorescence chlorophyll concentrations are five times higher than typical values away from the front (corroborated by analysis of bottle data, not shown). CTD data suggest that the chlorophyll anomaly extended to the depth of the mixed layer north of the front. Flow-through seawater line chlorophyll data, while not reaching the same high values as were observed in the CTD data, show high values extending to order 10 km to the north of the front. Laser induced chlorophyll fluorescence data from NASA aircraft (Yoder *et al.*, 1994), which should reflect the sea surface *Rhizosolenia* patch, revealed elevated values in a sharp front located at 2.5°N on 25 August, when most of the cold water CTD deployments were made (the warm side of the front was mostly sampled on the 26 August).

Profiles of chemical and biological properties from across the front are presented in Fig. 11. The profiles are resolved into warm and cold endmembers (from 3°N and 1°N, stations 5 and 7, respectively) and casts from near the front, divided by the sea surface temperature into warm and cold front casts (all from station 6 near 2°N). Most of the chemical impact of the front is seen on the warm side; the only apparent distinction between cold front and cold end-member casts in Fig. 11 is that σ_θ is somewhat higher at the sea surface close to the front (as noted previously, the cold front waters were the densest outcrop observed during the entire JGOFS Survey expeditions). On the warm side, some of the observed chemical properties from the front casts, notably σ_θ and NO_3, resemble a hybrid transition between the cold casts and the warm end-member, reflecting the layered structure of the water column north of the front. However, other properties are anomalous near the front. Specifically, warm frontal waters had extremely depressed pCO_2 (Archer *et al.*, 1996) and AOU (denoting oxygen supersaturation), and elevated values of TOC (Peltzer and Hayward, 1996) and POC relative to the warm endmember. These geochemical tracers are all indicative of high absolute rates of primary productivity.

Table 1. *Calculated deployment distances from the front of CTD deployments from Stations 5, 6, and 7 (nominally 3°N, 2°N and 1°N). From (Johnson, 1996)*

CTD	Latitude	Longtitude	Distance*	Corrected distance†
58	2.9217	−140.1583	129.84	
59	2.9050	−140.2100	127.08	
60	2.8850	−140.2433	125.37	
61	2.8700	−140.3100	105.73	
62	2.8550	−140.3350	123.04	
63	2.8283	−140.3733	119.88	
64	2.8233	−140.4117	120.12	
65	2.8167	−140.4367	120.25	
66	2.6067	−140.7783	113.12	
67	2.5983	−140.7850	111.50	
68	2.0933	−140.1917	−10.90	−10.83
69	2.1200	−140.2433	−10.02	−10.49
70	2.1300	−140.3033	−7.63	−8.42
71	2.1700	−140.3917	−2.47	−3.77
72	2.1650	−140.4367	−4.03	−5.81
73	2.2033	−140.5050	−0.31	−2.57
74	2.2083	−140.5467	−0.08	−2.69
75	2.1950	−140.6900	−5.72	−5.54
76	2.2067	−140.7033	−5.08	−4.83
77	2.2283	−140.7500	−3.02	−2.58
78	2.2700	−140.8650	1.97	3.16
79	2.2667	−140.8817	2.10	3.25
80	2.1150	−141.2683	8.25	
81	2.0933	−141.4350	2.38	
82	2.0867	−141.4383	0.79	
83	2.0850	−141.4467	0.03	
84	1.1067	−140.0050	−220.75	

*Calculated by assuming that the front can be described by a line moving to the west at a rate of 64.1 ± 2.4 cm s^{-1} with a direction of $315.6 \pm 4.5°$, located at a position of 2.2196°N, 140.7099°W, at 1608 GMT on 25 August 1992.

†Corrected based on the location of the front based on most recent ADCP sea surface temperature detection of the 25.5° isotherm.

Production within the warm frontal waters. Oxygen in the warm frontal mixed layer was roughly 45 μmol kg^{-1} supersaturated, while values in the warm end-member sea surface were near saturation. Using the Redfield respiration ratio, this oxygen signal translates to a removal of approximately 35 μM ΣCO_2 by photosynthesis in a closed system. The analogous calculation can be done using the patch anomaly in pCO_2, which was 65 μatm lower in the patch than in warm end-member casts. The deficit of dissolved CO_2 required to generate this observed deficit of pCO_2 can be approximated by:

$$\Delta \sum CO_2 = \gamma^{-1} \frac{\Delta pCO_2}{pCO_2} \sum CO_2$$

where γ is the Revelle buffer factor [assumed for the warm patch waters to be 8 (Archer *et al.*, 1996)], and taking $\Delta pCO_2 = 65$ μatm, $pCO_2 = 380$ μatm, and $\Sigma CO_2 = 1960$ μmol kg^{-1} (warm end-member values), we can calculate that approximately 40 μmol kg^{-1} ΣCO_2 must have been removed from the warm front water to the warm end-member, consistent with the oxygen anomaly in a closed system.

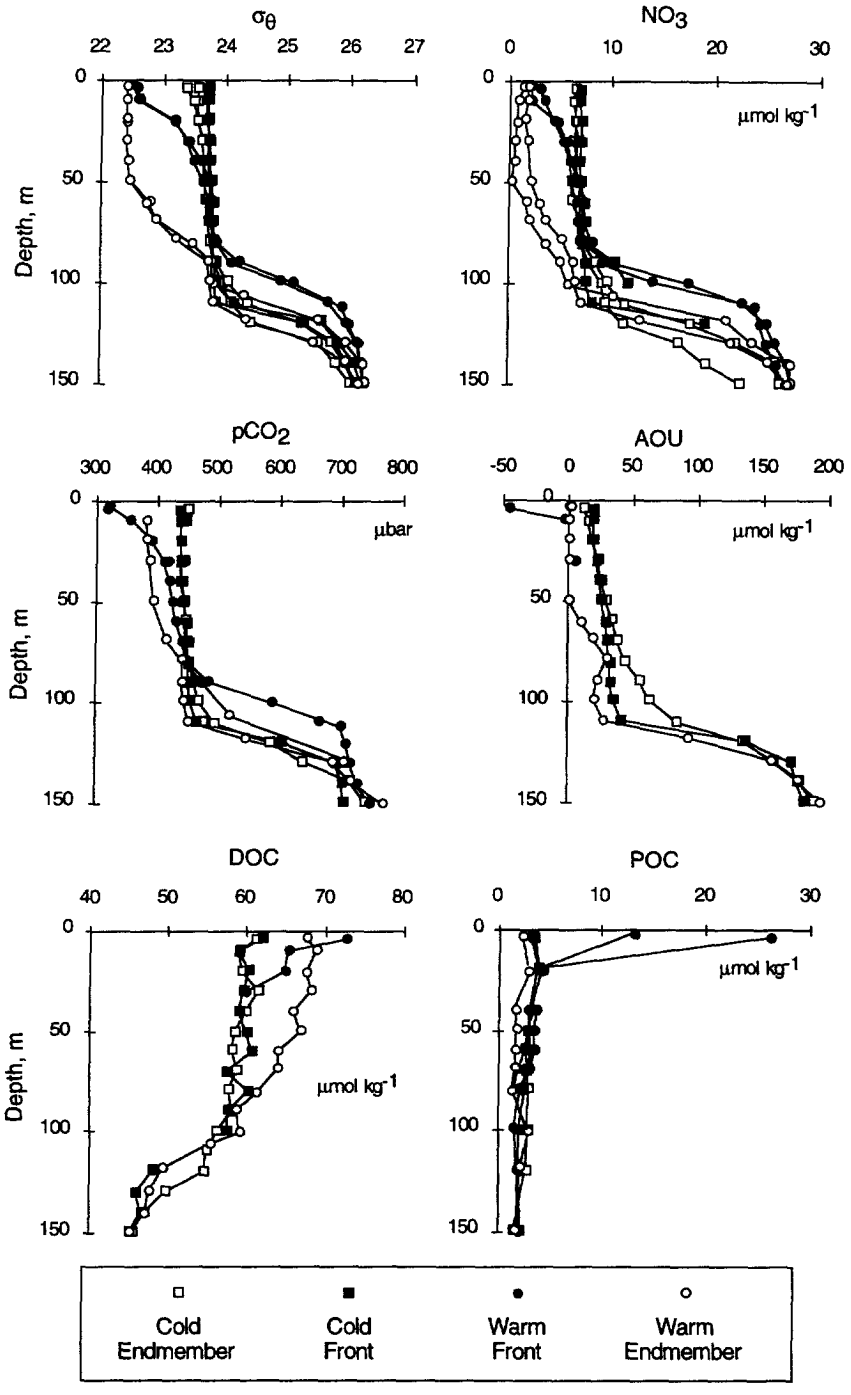

Fig. 11. Profiles of water properties resolved into warm and cold endmembers (station 5: 3°N, casts 58 and 65, open circles; station 7: 1°N, casts 84 and 89, open squares, respectively) and casts from near the front, divided by the sea surface temperature into warm and cold front casts (all from station 6 near 2°N, warm from casts 79 and 82, closed circles; cold from casts 68 and 74, closed squares). Data from Garside and Garside (1995), Archer *et al.* (1996) and Peltzer and Hayward (1996).

Oxygen supersaturation in surface waters has often been used as a measure of the rate of biological production as, for example, by Spitzer and Jenkins (1989). Assuming a gas exchange piston velocity of 3 m day^{-1}, the oxygen evasion rate from the warm frontal water to the atmosphere (neglecting the narrow patch zone) was approximately 140 mmol O_2 m^{-2} day^{-1}. However, it would be deceptive to make the usual assumption that the oxygen degassing flux is equivalent to the biological source flux. Gas exchange would fractionate O_2 and CO_2 if it were the dominant balance for biological production (see Archer *et al.*, 1996 and caption to Fig. 6). Here we observed no fractionation; both O_2 and CO_2 anomalies from warm end member chemistry indicate a removal of approximately 35–40 μM ΣCO_2. We propose two potential explanations. The first possibility is that the time scale of the biological perturbation was shorter than the gas exchange time. For example perhaps a day–night cycle in photosynthesis and respiration generated oxygen supersaturation only during the day time. However, this hypothesis would predict a greater day–night cycle in pCO_2 than was detected in the continuous pCO_2 data (Goyet and Peltzer, submitted).

The second possibility is that the waters in the warm frontal waters are quickly flushed by turbulent mixing and subduction, a process which would not fractionate between O_2 and CO_2 (the flushing hypothesis). The gas exchange time scale was of order 5 days, assuming a mixed layer thickness of 16 m and a gas exchange rate constant of 3 m d^{-1}; the flushing hypothesis would imply that the residence time for warm frontal water must be shorter than this. A physical analysis of the front support the flushing hypothesis (Johnson, 1996). The dynamics of gravity flows predict mixing at a turbulent hydraulic jump just to the warm side of the front. Also, the residence time of warm frontal water can be estimated from ADCP and CTD data on either side of the front. On the south (cold) side, northward water flow into the front is restricted to a very narrow density range, reflecting the fact that the surface waters are well mixed. On the north side, the mass flux nearly balances the flux south of the front, but the density range of the flowing water has widened, presumably by mixing and subduction of warm waters into the cold flow beneath. Heat balance requires a southward flux of warm water of approximately 1.0 m^3 s^{-1} m^{-1} length of the front. This warm water flux implies a residence time for water in a patch 16 m deep and 8 km wide (the distance from the front of the CTD profile used by Johnson) of about 2 days.

The implication of the short residence time for warm frontal water coupled with the oxygen and CO_2 anomalies is that oxygen production rate within the warm frontal water may have been many times higher than the 140 mmol m^{-2} d^{-1} calculated above. Assuming a mixing time of 2 days and a water slab thickness of 16 m, a production rate of very roughly 300 mmol m^{-2} d^{-1} within the patch would be required to maintain the observed oxygen or CO_2 anomalies. However, this estimate is sensitive to the depth distributions of oxygen anomaly and water residence time (flow), neither of which are well resolved in the data.

Particles in the warm frontal water. The concentration of particulate organic carbon (POC) in the bulk mixed layer on the warm side of the front was elevated to approximately 13–26 μmol kg^{-1} (two replicates) relative to typical sea surface values away from the front of 2–3 μmol kg^{-1}. Thus, a considerable extent of the biological perturbation of O_2 and CO_2 could be accounted for simply by production of organic matter which remained suspended in the patch mixed layer. The problems with this simple scenario are the NO_3, PON and ^{234}Th data. The biological production implied by the CO_2 and O_2 data corresponds to approximately 5 μmol kg^{-1} of nitrogen (the measured particle C/N within the warm frontal water was 5.64). However, we notice that the warm end-member surface contained only

about 1.5 μmol kg^{-1} NO_3, the dominant form of available dissolved nitrogen and that values in the patch waters were, in fact, actually somewhat higher than this (2–3 μmol kg^{-1}). Since the required nitrogen to produce the PON is greater than the total dissolved concentration in warm end-member waters, we must conclude there are other ways of importing fixed N to that water parcel. One possibility is nitrogen fixation within the patch, but this would require very high rates in the presence of dissolved NO_3, which seems unlikely. Another possibility is that the nitrogen was imported in particulate form, floating out of subducting cold waters from the south, as concluded by (Yoder *et al.*, 1994). *Rhizosolenia* sp. mats in the north Pacific have, in fact, been observed vertically transporting NO_3 (Villareal *et al.*, 1993, 1996), although this was in nutrient depleted conditions.

At the same time, although uptake of NO_3 appears to be an insignificant term in the PON budget, the anomalies in dissolved oxygen and CO_2 argue that a considerable excess of photosynthesis over respiration must have taken place within the waters of the patch. Our conclusion must be that the *Rhizosolenia* carry enough metabolic nitrate from their previous residence in the nitrate-rich equatorial waters that exposure to sunlight allows considerable uptake of CO_2 and release of oxygen by photosynthesis without further uptake of nitrogen (again consistent with Villareal *et al.* (1993, 1996)). Regardless of the uncertain time-dependent behavior and turbulent mixing regime, the observed anomalies in solute chemistry insist that this uncoupling between carbon and nitrogen must have occurred.

The conclusion that particles were imported to front waters is also supported by measurements of ^{234}Th within the waters of the front. ^{234}Th is produced by the decay of ^{238}U, which has an activity of 2.40 dpm kg^{-1} in ocean waters. In a closed system steady state, the activity of ^{234}Th would equal the activity of ^{238}U (secular equilibrium). In surface waters, the activity of ^{234}Th is typically observed to be lower than this, because some Th is scavanged by sinking particles. Surface waters away from the front between 1–3°N contained 1.4–2.15 dpm kg^{-1} of ^{234}Th total (dissolved plus particulate), while waters from a CTD cast approximately 3 km on the warm side of the front contained a total of 3.3 dpm kg^{-1}; actually higher than the secular equilibrium value. This is strong evidence for the import of particles bearing ^{234}Th to the front water. Also, dissolved ^{234}Th, a signature of redissolving particles, was not anomalously high in the front. This is consistent with the conclusion based on dissolved O_2 and CO_2, above, that a water parcel within the front had only a short residence time (less than 3 days) before subduction.

SUMMARY

The JGOFS Survey II expedition crossed through a convergent front at 2°N during August 1992. The front was the leading edge of a tropical instability wave and separated cold equatorial water to the south from the warmer equatorial counter current water to the north. Signatures of subduction can be seen below the warm water north of the front, and a patch of buoyant phytoplankton accumulated in the convergence zone.

Disequilibrium of surface waters with atmospheric oxygen concentration was seen on both sides of the front: undersaturation in cold waters to the south and supersaturation in patch waters adjacent to the front to the north. The undersaturated waters to the south were apparently the product of recent exposure of sub-surface waters to the atmosphere. Based on the depth of mixing and the rate of gas exchange, we estimate that this water had only been exposed for 10–20 days. These waters had elevated concentrations of dissolved organic carbon relative to waters of the same density but below the surface during Survey I, indicating that DOC production occurred quickly in response to exposure to sunlight. The

T/S signature of surface waters south of the front could be traced sub-surface 100 km north of the front; these waters contained high concentrations of NH_4 relative to Survey I results, presumably the product of subduction and oxidation of suspended organic matter.

The warm waters at the line of convergence were filled with buoyant *Rhizosolenia* sp. phytoplankton. The dynamics of fluid and particles within the *Rhizosolenia* patch are constrained by observations and budget calculations for the biological tracers O_2, CO_2, chlorophyll and fixed nitrogen. A nitrate budget and thorium data indicate that much of the standing stock of particulates must have been imported as particles rather than growing in place. However, the concentrations of O_2 and CO_2 were both perturbed from source values, indicating that primary production had occurred within patch waters, but apparently without corresponding NO_3 uptake (an uncoupling of normal Redfield stoichiometry). The oxygen and CO_2 anomalies are of comparable (Redfield) magnitudes, which probably indicates that the biological source for O_2 by photosynthesis was balanced by turbulent mixing and subduction of front waters (which would not fractionate the two gases) rather than gas exchange (which would fractionate). This conclusion is supported by dissolved ^{234}Th. The implication of this is that the residence time for patch water was only a few days.

REFERENCES

Aiken, J. and Bellan, I. (1990) Optical oceanography: an assessment of a towed method. In *Light and Life in the Sea*, ed. P. J. Herring, A. K. Campbell, M. Whitfield and L. Maddock, pp. 39–57. Cambridge University Press, Cambridge.

Archer D. E., Peltzer, E. and Kirchman, D. (1997) A time scale for DOC production in equatorial Pacific surface waters. *Global Biogeochemical Cycles*, **11**, 435–452.

Archer, D. E., Takahashi, T., Sutherland, S., Goddard, J., Chipman, D., Rodgers, K. and Ogura, H. (1996) Daily, seasonal, and interannual variability of sea surface carbon and nutrient concentration in the equatorial Pacific Ocean. *Deep-Sea Research II*, **43**, 1155–1180.

Balch, W. M. and Kilpatrick, K. (1996) Calcification rates in the equatorial Pacific along 140°W. *Deep-Sea Research II*, **43**, 971–994.

Barber, R. T., Sanderson, M. P., Lindley, S. T., Chai, F., Newton, J., Trees, C. C., Foley, D. G. and Chavez, F. P. (1996) Primary production in the equatorial Pacific along 140°W. *Deep Sea Research II*, **43**, 933–970.

Beebe, W. (1926) *The Arcturus Adventure*. The Knickerbocher Press, New York, 433 pp.

Flament, P., Kennnan, S., Knox, R., Niiler, P. and Bernstein, R. (1996) The three-dimensional structure of a tropical instability wave. *Nature*, **383**, 610–613.

Garside, C. and Garside, J. C. (1995) Euphotic zone nutrient algorithms for the NABE and Eqpac study sites. *Deep-Sea Research II*, **42**, 335–348.

Goyet C. and Peltzer, E. T. (submitted) Variation of CO_2 partial pressure in surface seawater in the equatorial Pacific Ocean. *Deep-Sea Research II*.

Harrison, D. E. (1996) Vertical velocity in the central tropical Pacific—a circulation model prespective. *Deep-Sea Research II*, **43**, 687–706.

Johnson, E. S. (1996) A convergent instability wave front in the central tropical Pacific. *Deep-Sea Research II*, **43**, 753–778.

Kessler, W. S. and McPhaden, M. J. (1995) The 1991–1993 El Nino in the central Pacific. *Deep-Sea Research II*, **42**, 295–334.

Legeckis, R. (1977) Long waves in the eastern equatorial Pacific: a view from a geostationary satellite. *Science*, **197**, 1177–1181.

McCarthy, J. J., Garside, C., Nevins, J. and Barber, R. T. (1996) New production along 140°W in the equatorial Pacific during and following the 1992 El Nino event. *Deep-Sea Research II*, **43**, 1065–1094.

McPhaden, M. (1996) Monthly period oscillations in the Pacific north equatorial countercurrent. *Journal of Geophysical Research*, **101**, 6337–6359.

Murray, J. W., Johnson, E. and Garside, C. (1995) A U.S. JGOFS process study in the equatorial Pacific (EQPAC): introduction. *Deep-Sea Research II*, **42**, 275–294.

Peltzer, E. T. and Hayward, N. A. (1996) Spatial and temporal variability of total organic carbon along 140°W in the equatorial Pacific ocean in 1992. *Deep-Sea Research II*, **43**, 1155–1180.

Sawyer, M. and Flament, P. (1995) A three-dimensional view of the equatorial front. *Deep-Sea Research (cover)*, **42**, 00.

Spitzer, W. S. and Jenkins, W. J. (1989) Rates of vertical mixing, gas exchange, and new production: estimates from seasonal gas cycles in the upper ocean near Bermuda. *Journal of Marine Research*, **47**, 169–196.

Villareal, T. A., Altabet, M. A. and Culver-Rymsza, K. (1993) Nitrogen transport by vertically migrating diatom mats in the north Pacific Ocean. *Nature*, **363**, 709–712.

Villareal, T. A., Woods, S., Moore, J. K. and Culver-Rymsza, K. (1996) Vertical migration of *Rhizosolenia* mats and their significance to NO_3 fluxes in the central north Pacific gyre. *Journal of Plankton Research*, **18**, 1103–1121.

Welling, L. A., Pisias, N. G., Johnson, E. S. and White, J. R. (1996) Distribution of polycystine radiolaria and their relation to the physical environment during the 1992 El Nino and following cold event. *Deep-Sea Research II*, **43**, 1413–1434.

Wyrtki, K. (1981) An estimate of the equatorial upwelling in the Pacific. *Journal of Physical Oceanography*, **11**, 1205–1214.

Yoder, J. A., Ackleson, S. G., Barber, R. T., Flament, P. and Balch, W. M. (1994) A line in the sea. *Nature*, **371**, 689–693.

Zhang, X., Dam, H. D., White, J. R. and Roman, M. R. (1995) Latitudinal variations in mesozooplankton grazing and metabolism in the central tropical Pacific during the EqPac study. *Deep-Sea Research II*, **42**, 695–714.